RSC Advances

PAPER

View Article Online
View Journal | View Issue

Cite this: *RSC Adv.*, 2024, **14**, 12873

Efficient dye adsorption of mesoporous activated carbon from bamboo parenchyma cells by phosphoric acid activation†

Yuxuan Yao,‡[ab] Haifeng Zuo,‡[ab] Yijing Liu,[ab] Shenghua Pang,[ab] Liuqian Lan,[ab] Futi Yao,[ab] Yongyi Wu[ab] and Zhigao Liu *[ab]

Received 3rd March 2024
Accepted 15th April 2024

DOI: 10.1039/d4ra01652a

rsc.li/rsc-advances

In order to solve the environmental damage caused by the discharge of dyes as industrial wastewater, the development of efficient and sustainable adsorbents is the key, while most of the previous studies on bamboo parenchyma cells have focused on their microstructural, functional and mechanical properties, and few of the properties in adsorption have been investigated. To evaluate the role of the unique microstructure of bamboo parenchyma cells on adsorption after carbonization and activation, PC-based activated carbon (PPAC) was fabricated by the phosphoric acid activation method and tested for adsorption using methylene blue (MB). The effect of mesoporous structure on MB adsorption was investigated in detail using PPAC-30C impregnated with phosphoric acid at a concentration of 30%. The results showed that the adsorption performance was influenced by single-factor experiments (*e.g.*, pH, activated carbon dosing). The adsorption isotherms and kinetics could conform to the Langmuir model (R^2 = 0.983–0.994) and pseudo-second-order kinetic model (R^2 = 0.822–0.991) respectively, and the maximum MB adsorption capacity of adsorbent was 576 mg g^{-1}. The adsorption mechanism of MB on PPAC-30C includes physical adsorption, electrostatic attraction, hydrogen bonding, and the π–π conjugation effect, which was dominated by physical adsorption. The results of this study show that PPAC has good application prospects for cationic dye removal.

1. Introduction

Water, as one of the important substances to maintain the survival of life, is inextricably intertwined with human production, life, and even social development. Global freshwater scarcity has been further exacerbated in recent decades by climate change, population growth, and water pollution that causes severe water shortages for at least one month each year for about 4 billion people.[1] Dye pollution is stable and difficult to degrade, in additional to imparting colour to water bodies, preventing sunlight penetration, and disrupting the ecology of water bodies.[2] Methylene blue (MB), a typical cationic azo dye, is one of the most commonly used materials in the dye industry.[3] It has a wide range of uses, in addition to being used for the colourings of silk, wool, cotton and paper, it is also used as a redox indicator in the chemical field.[4,5] Research into the safe treatment of MB is of great practical importance due to its toxicity, carcinogenicity, and non-biodegradability.[6]

Currently, typical methods for dye removal include photocatalytic degradation, biodegradation, reverse osmosis, ion exchange, chemical/electrochemical oxidation, and adsorption.[7–9] Adsorption is a cost-effective and efficient method that is simple to operate and produces no toxic by-products during treatment, making it a method offers a wide range of potential applications.[10] Carbon-based materials valued for high performances and multifunctionality,[11,12] although various adsorbents such as carbon nanotubes,[13] hydrogels[14] and nanofibers[15] have been prepared and used for the removal of dyes from water, activated carbon is a widely utilized as industrial adsorbent due to its highly developed pore structure, high specific surface area, and abundance of functional groups.[16] The production of activated carbon cannot be done without high carbon content substances as precursors, and since fossil fuels are in short supply, biomass resources as raw materials have become a better choice.[17,18] Bamboo, of which has been noticed for its fast growth, short felling period, high strength and strength, and excellent fracture toughness.[19,20]

The composition of bamboo mainly consists of fibre and parenchyma cells, with a slightly higher proportion of parenchyma cells. Bamboo is an excellent material for various industries due to its high strength-to-weight ratio. Its fibres

[a]*School of Resources, Environment and Materials, Guangxi University, Nanning 530000, Guangxi Zhuang Autonomous Region, China. E-mail: lzgk18@gxu.edu.cn*
[b]*State Key Laboratory of Featured Metal Materials and Life-cycle Safety for Composite Structures, Guangxi University, Nanning 530004, China*

† Electronic supplementary information (ESI) available. See DOI: https://doi.org/10.1039/d4ra01652a

‡ Yuxuan Yao and Haifeng Zuo contributed equally to this work as co-first authors.

have been used in the paper industry for over 1700 years and are now also utilized in the textile and construction industries.[21] In recent decades, parenchyma cells have received increasing attention, however, most of the related studies have focused on their microstructure and mechanical properties.[19,22] As a biomaterial with a natural multilayered microcapsule-like structure, the effect of its unique microstructure on adsorption after carbonization and activation is still poorly understood. Xia *et al.* (2023) found that after further activation, the PCs could still maintain complete cell morphology and multilayer structure and he took full advantage of this to prepare highly porous KOH activated carbon with an adsorption value of up to 1750 mg g^{-1} for MB.[10] It is particularly important to investigate the adsorption mechanism of cationic dyes on bamboo parenchyma cell activated carbon under different activation conditions, and to explore the development of its pollution control capability and the high-value use of bamboo parenchyma cells, given the very high potential of bamboo parenchyma cell activated carbon for energy storage and removal of cationic dyes. As far as activators are concerned, phosphoric acid catalyses the elimination of hydroxyl groups in organic compounds and can be further combined with raw materials to produce phosphate esters and polymerization products of phosphoric acid.[23] For biomass materials such as bamboo parenchyma cells with high cellulose content, phosphoric acid activated carbon has a higher proportion of mesopores and is more suitable for adsorption of MB molecules.[24–26]

In summary, the phosphoric acid-activated bamboo parenchyma cells based activated carbon was used in this paper to investigate its adsorption performance on MB. Different phosphoric acid impregnation concentration samples of activated carbon were prepared to investigate the adsorption of MB. To investigating the adsorption mechanism of MB on activated carbon with mainly mesopores, this paper did not adopt the PPAC-10C with the highest adsorption capacity, but chose the PPAC-30C with rich mesopores as the main object of study. The adsorption kinetics, adsorption thermodynamics and ionic interference experiments were carried out and finally the adsorption mechanism was revealed.

2. Materials and methods

2.1. Materials

Bamboo samples was taken from Hangzhou, Zhejiang Province. All chemical reagents were used as received for the experiment without further purification and deionized water was used throughout the experiments. Sodium chlorite ($NaClO_2$) was obtained from Shanghai Maclean Biochemical Technology Co., Ltd. Disodium hydrogenphosphate (Na_2HPO_4) was purchased from Tianjin Beichen District Fangzheng Reagent Factory. Potassium sulphate (K_2SO_4, ≥99%), acetic acid (CH_3COOH, 99.5%), and potassium hydroxide (KOH, 90%) were purchased from Chengdu Kolon Chemical Co., Ltd. Potassium dihydrogen phosphate (KH_2PO_4, ≥99.5%) and phosphoric acid (H_3PO_4, ≥99%) were purchased from Chengdu Jinshan Chemical Reagent Co. Methylene blue (MB), methyl orange (MO), tripotassium phosphate (K_3PO_4, ≥99%), ofloxacin (OFLX), and ciprofloxacin (CIP) were sourced from Shanghai Maclean Biochemical Technology Co., Ltd. Magnesium chloride ($MgCl_2$, ≥99%) and potassium chloride (KCl) were purchased from Tianjin Opusheng Chemical Co.

2.2. Preparation of bamboo parenchyma cells

The separation process was carried out according to the method described in our previous study (Xia *et al.* 2023) and the whole flowchart of the experiment is shown in Fig. 1.[10] The moso bamboo was cut into 100 mm length × 10 mm width × 2 mm, placed in a crystallization dish, and immersed in 1% $NaClO_2$ solution, then the pH of the mixed solution was adjusted to 4.5–4.6 with CH_3COOH, followed by heating in a water dish to 80 °C and changing the solution every 6 hours. The above procedure was repeated until the strips became completely white. The whitened strips were washed with deionized water until neutral. They were then dried in a freeze dryer for 72 hours. The ground tissue of a culm consists of parenchyma cells, with embedded vascular bundles composed of metaxylem vessels, sieve tubes with companion cells, and fibres. On an average, a culm consists of about 52% parenchyma cells and 40% fibres.[27] After drying, the white powdery substance can be collected by gentle shaking. After passing through a 100-mesh sieve, the powder was collected as bamboo parenchyma cells (PCs) and transferred to a desiccator for storage.

2.3. Preparation of phosphoric acid activated PCs-based activated carbon

5 g of bamboo parenchyma cell powder was accurately weighed into a beaker and 30 ml of phosphoric acid at various levels of 10%, 30% and 50% was measured and mixed with it. After proper stirring, the samples were stirred at 500 rpm for 1 hour at room temperature for complete maceration. The blended samples were dried in an oven at 80 °C to constant weight. The mixed samples were then put into a tube furnace and heating up to 500 °C at 8 °C min^{-1} at a nitrogen flow rate of 150 ml min^{-1} for 1 hour and then reduced to room temperature. At last, it was cleaned with deionized water until neutral. These activated carbon samples were named PPAC-10C, PPAC-30C and PPAC-50C respectively.

2.4. Batch adsorption

2.4.1 Factors impacting adsorption performance. The MB dye solution was mixed with PPACs in a 50 ml Erlenmeyer flask

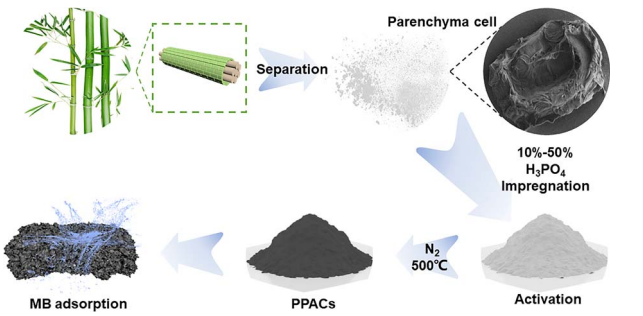

Fig. 1 Overall experimental flow chart.

and three batch adsorption experiments were carried out. The study investigated the relations between the factors affecting the adsorption performance of MB, such as adsorbent dose (0.1–0.8 g L^{-1}), pH (1–13), specified contact time (0–2000 min) and temperature (adjusted to 25, 35 and 45 °C). Table 1 shows the specific experimental conditions. Immediately after performing the tests on a 180 rpm thermostatic water bath oscillator, a sample of the mixture was extracted from the Erlenmeyer flask of each batch using a disposable syringe. A polyether sulfone filter (0.45 μm) was then applied to the extracted samples. A UV-5500 spectrophotometer (UV-5500, Shanghai Yuan Analytical Instruments Corporation, China) was used to measure the absorbance of the supernatant at 665 nm. To evaluate the adsorption effect of MB in the adsorption experiments, the concentration of the supernatant was calculated using the standard curve method. The average of three measurements was taken for all adsorption experiments. The kinetics and thermodynamics were fitted by means of a non-linear fit model. The equilibrium amount of the adsorbed dye (Q_e) and the dye removal rate at equilibrium were evaluated by using the eqn (1) and (2):

$$Q_e = \frac{(C_0 - C_e)V}{M} \quad (1)$$

$$R_e = \frac{(C_0 - C_e)}{C_0} \times 100\% \quad (2)$$

where V (L) is the volume of MB solution; M (g) is the mass of PPAC-30C; the initial and equilibrium concentrations of MB are expressed as C_0 and C_e (mg L^{-1}), respectively.

2.4.2 Batch adsorption experiments. Except batch test III, all the batch adsorption experiments used 20 mg PPAC placed in conical flasks containing MB solution of different initial concentrations and volume and adsorbed at 180 rpm for 20 h. In order to investigate the effect of PPAC as adsorbent material on the removal of dyes under different activation conditions, Batch Test I was carried out using methylene blue as the pollutant. Batch Test II was conducted to investigate the effect of initial pH on adsorption performance. Batch Test III was conducted to investigate the effect of activated carbon dosage on adsorption performance. PPAC-30C was added to a conical flask containing methylene blue solution (20 ml, 300 mg L^{-1}, pH = 7, 298 K), keeping the volume of methylene blue solution constant, varying the mass of activated carbon dosing, controlling the dosage and adsorbing at 180 rpm for 20 h.

To study the adsorption kinetics, the Batch Test VII was carried out. 20 mg PPAC-30C was added to a conical flask containing five different initial concentrations (100 mg L^{-1}, 200 mg L^{-1}, 300 mg L^{-1}, 400 mg L^{-1}, 500 mg L^{-1}) of MB solution (40 ml, pH = 7) and shaken at 180 rpm for 24 h at 298 K. At certain time points, the MB concentration was determined.

Isothermal adsorption experiments include Batch Test IV, V and VI at ambient temperatures of 298 K, 308 K and 318 K, respectively. 20 mg PPAC-30C was placed in conical flasks containing different initial concentrations of MB solution (40 ml) and adsorbed at 180 rpm for 20 h. Detailed parameters of each temperature batch are given in Table 1.

2.5. Competitive adsorption

To investigate the effect of co-existing anion (Cl^-, SO_4^{2-}, PO_4^{3-}) and cation (K^+, Na^+, Mg^{2+}) on the adsorption performance of MB, 20 mg of PPAC-30C was added to 40 ml of a mixed solution of MB (300 mg L^{-1}) and different anion and cation, where the ion concentrations were 0 mol L^{-1}, 0.002 mol L^{-1}, 0.006 mol L^{-1}, 0.01 mol L^{-1}. The pH of the mixed solution system was adjusted to 7 with 0.1 M HCl and agitated at 180 rpm for 20 h at 298 K.

2.6. Characterization

A detailed list of the methods used for the characterization of all the samples can be found in TEXT S1 (ESI File).†

3. Results and discussion

3.1. Pore structure analysis

The N_2 adsorption/desorption curves of PPACs at the various impregnation levels were shown in Fig. 2(a). At relatively weak pressure, the N_2 adsorption of the activated carbon samples increased sharply, indicating the presence of many microporous structures in the samples.[28] As the impregnation concentration increased, the isotherms shifted from Type I to Type IV

Table 1 Adsorption experimental parameters and conditions

		Experimental condition			
		Adsorbent dosage (g L^{-1})	MB concentration (mg L^{-1})	pH	Temperature (K)
Batch test I	PPAC-10C PPAC-30C PPAC-50C	0.4	300	7	298
Batch test II	PPAC-30C	0.5	300	1,3,5,7,9,11,13	298
Batch test III	PPAC-30C	0.1,0.2,0.4,0.8	300	7	298
Batch test IV	PPAC-30C	0.5	100–500	7	298
Batch test V	PPAC-30C	0.5	100–500	7	308
Batch test VI	PPAC-30C	0.5	100–500	7	318
Batch test VII	PPAC-30C	0.5	100–500	7	298
Ion interference	PPAC-30C	0.5	300	7	298

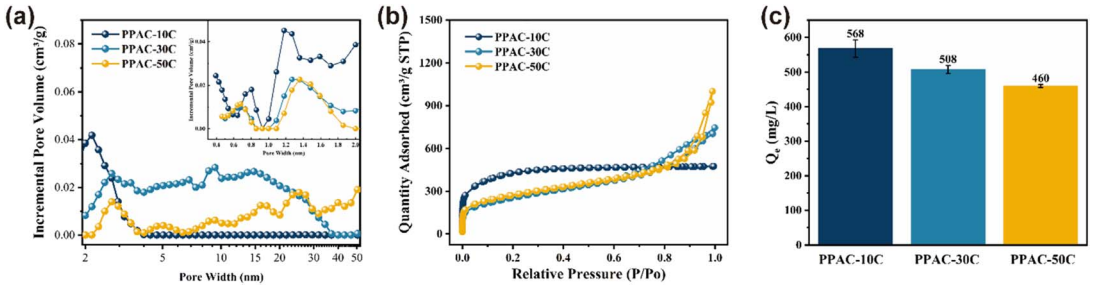

Fig. 2 Pore size distributions (a), N_2 adsorption/desorption isotherms (b), and MB adsorption capacity by PPACs (c).

according to the IUPAC taxonomy, showing the transition of the PPAC from a microporous-dominated pore structure to a mesoporous one.

Table S1† shows the pore size parameters of different PPACs. As can be seen from the table, the PPAC-10C sample has the highest specific surface area at different impregnation concentrations and has an average pore size of 1.921 nm, which demonstrates that the sample structure was dominated by micropores, which was consistent with the analysis in Fig. 2(a). In addition, the mesopore pore volume of the samples increased significantly with rising impregnation concentration, likely reflecting the higher phosphate concentration, and increased longer phosphate aggregates formed, thus diminishing the micropores and increasing the mesopores. Under high temperature (>300 °C) and anhydrous atmosphere, the oxide phosphorus pentoxide generated from phosphoric acid when the impregnation ratio was small can act as a Lewis acid, reacting to form C–O–P conjugated structure, and obtaining activated carbon with well-developed micropores and high specific surface area. The reaction formula was shown in Fig. 3.[29] Fig. 2(a) shows that the activated carbon samples have a wide distribution of mesopores, PPAC-30C having the widest distribution of mesopores, and this widespread mesopore structure was favourable for the attachment of MB molecules. Fig. 2(b) shows that with the increase of phosphate impregnation concentration, the isotherm type changes from type I isotherm of PPAC-10C to type II isotherm of PPAC-30C, PPAC-50C. The type I isotherm confirms the richness of microporous properties of PPAC-10C. The inflection points of the isotherms of PPAC-30C, PPAC-50C were in the low P/P_0 region, which indicates the completion of the adsorption of the monomolecular layer. The number of layers increases with the relative pressure, and when $P/P_0 = 1$, the platform is still not formed, indicating that the adsorption has not reached saturation, and it seems to be able to increase indefinitely. This isotherm type somehow indicates that the pore size type of activated carbon changes to be dominated by mesopores and macropores after the increase of phosphoric acid impregnation concentration.

3.2. Effect of PPACs prepared at different impregnation concentrations on MB removal

Fig. 2(c) illustrates the variations in the adsorption of MB by PPACs at different concentrations of phosphoric acid impregnation. It is evident from Fig. 2(c) that there are differences in

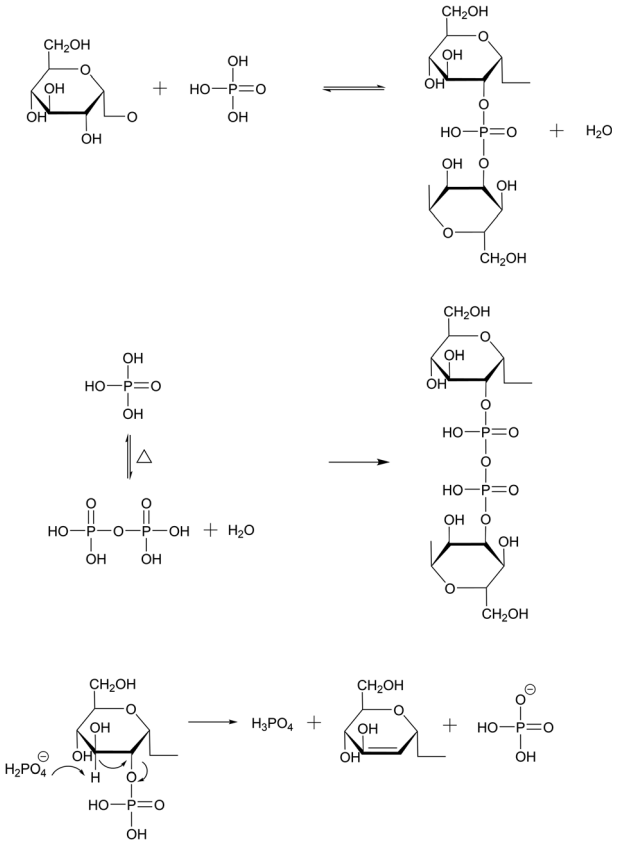

Fig. 3 Mechanism of phosphate ester formation after phosphorylation of cellulose.

the adsorption of MB by PPACs prepared with varying phosphoric acid impregnation concentrations. PPAC-10C has the highest adsorption capacity for MB, which may be attributed to its higher specific surface area. However, to investigate the effect of mesopores on MB adsorption, PPAC-30C was used as a subsequent adsorption experiment due to its higher adsorption capacity than PPAC-50C and the highest specific surface area of the mesopore (Table S1†).

3.3. Environmental application of the PPAC-30C for MB removal

The changes in the adsorption value of MB at different pH values were studied since the pH of the solution is an important

parameter affecting the adsorption effect. With progressive increase in pH, the adsorption value of MB by PPAC-30C showed a tendency to decrease and then increase (Fig. 4(b)). The pH of the solution was closely related to the presence of MB in aqueous solution. When the solution was acidic, MB was mainly in the molecular form, and as the pH of the solution increased, MB was gradually converted to the cationic form, and the MB^+ content in the solution gradually increased. The zero-point charge of PPAC-30C was 1.35 according to Fig. 4(a). At a solution pH $\leq$ 1.35, oxygenated functional groups on the activated carbon surface may be protonated, resulting in a positively polarized surface of the PPAC-30C, and the excess H^+ and H_3O^+ ions may compete for adsorption of the MB cations (MB^+), leading to a lower MB adsorption amount.[30] With increasing pH, the MB^+ content in the solution gradually increased and the binding of MB to PPAC-30C increased under the electrostatic effect. According to the above pore structure analysis results, PPAC-30C has a rich mesoporous structure, and many MB molecules enter the internal pores of PPAC-30C mainly through the pore filling effect under acidic conditions.[31,32] The competition between dye cations and protons for effective adsorption sites decreases with increasing pH. At simultaneously, the deprotonation of the hydroxyl and carboxyl functional groups released more adsorption sites, and electrostatic attraction between the negative charges on the activated carbon-surface and the dye cations was generated, facilitating the adsorption of MB.[33,34]

To examine the association between the adsorption of MB by PPAC-30C and the dosage of activated carbon, the adsorption behaviour, and the removal rate of MB at different dosages of PPAC-30C were investigated. As illustrated in Fig. 4(c), as the dosage of activated carbon increased, the adsorption of MB showed an obvious decreasing trend from 599 mg g^{-1} to 300 mg g^{-1}, while the removal rate steadily improved from 20% to 100%, which can be traced to the increase in active sites and the ability of MB molecules to combine with the active points as the dosage of activated carbon increased.[35] On the other hand, when the original MB content is the same, increasing the activated carbon dosage decreases the average amount of MB that can be adsorbed within a unit of adsorbent.

3.4. Adsorption kinetics

Fig. 4(d) shows the MB solution adsorption profiles of PPAC-30C samples at different initial concentrations as a function of time. When the adsorption process started, the activated carbon had the most adsorption sites and the highest mass transfer capacity, so the PPAC-30C quickly entered the adsorption phase.

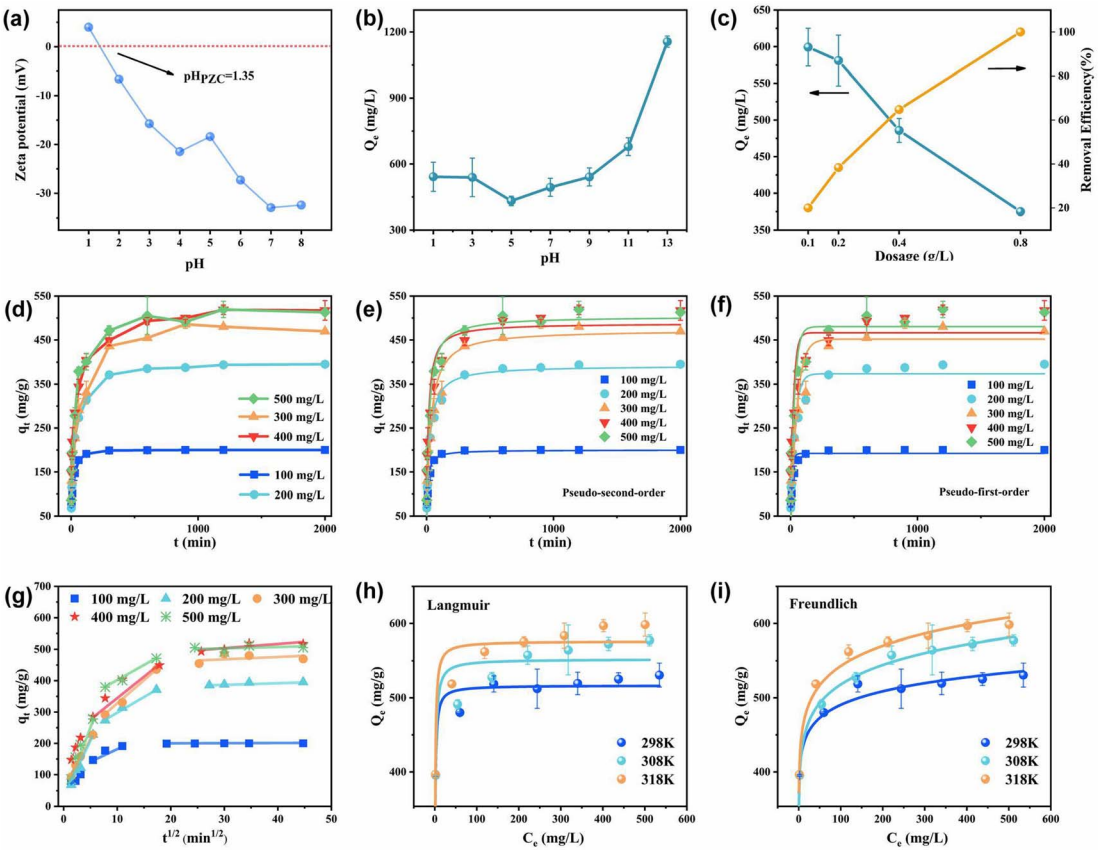

Fig. 4 The zero-charge point (a); initial pH (b); adsorbent dosage (c) on the MB removal capability by PPC-30C; effect of contact time (d); pseudo-first-order kinetic non-line model (e); pseudo-second-order kinetic non-line model (f); intra-particle diffusion model (g) for adsorption by PPAC-30C at different concentrations (pH = 7, T = 298 K, adsorbent dosage = 0.5 g L^{-1}); fitting of Langmiur non-linear model for PPAC-30C (h); fitting of Freundlich non-linear model for PPAC-30C (i).

The amount of PPAC-30C adsorbed increased with time until the active sites were gradually occupied, causing the rate of adsorption to slow down, with equilibrium being reached after approximately 300 to 600 min. The adsorption of methyl bromide on PPAC-30C at different initial concentrations showed the same trend, but with the increase of initial concentration, the time point for PPAC-30C to reach adsorption equilibrium was gradually delayed from 2 h to 5–10 h. During the adsorption process, the original active binding sites of the activated carbon were gradually reduced, leading to an increase in the electrostatic repulsive force between the ions, which eventually resulted in the adsorption reaction reaching a state of equilibrium.

As shown in Table S2,† the fitted R^2 of the pseudo-second-order kinetic model for the adsorption of MB on PPAC-30C at varying initial concentrating was higher than that of the pseudo-first-order kinetic model, and the equilibrium adsorption quantities, $q_{el,cal}$, derived by the pseudo-second-order kinetic model were more similar to the experimental values. This implies that the pseudo-second-order kinetic model can better explain all the adsorption processes of MB on PPAC-30C involving electrostatic attraction, ion–exchange interactions and π–π bonding.[36,37] The pseudo-second-order kinetic parameter k_2 gradually decreased from 0.00075 to 0.00010 with the initial concentration of MB solution increased, suggesting that the adsorption process was more favourable, which was mainly due to the increase in mass transfer motive force with the solution concentration growth. Similar results were reported for some dye-adsorbent systems.[38,39]

The fitting of the intra-particle diffusion model to the adsorption process of MB on PPAC at different concentrations was shown in Fig. 4(f). From the Fig. 4(f), the nonlinear adsorption process of MB on PPAC-30C at different concentrations can be divided into three parts throughout the adsorption process. The three linear processes were fitted into a straight line, and their slopes were the adsorption rate constants of the stage, which were denoted as k_{id1}, k_{id2}, and k_{id3}, respectively. The results showed that there existed a quantitative relationship of $k_{id1} > k_{id2} > k_{id3}$ between the three stages. The first stage was the fast adsorption stage, when the particles diffuse rapidly from the edge of the material to the outer surface at a rate controlled by membrane diffusion. The second stage was the diffusion of MB molecules from the surface of the adsorbent to the internal pores, and the rate of this step was limited by intra-particle diffusion. The third phase was the plateau phase, which represents the adsorption equilibrium. The intercepts of the adjusted intra-particle diffusion plots for different MB molecule concentrations were all non-zero, showing that intra-particle diffusion was not the exclusive influencing factor and that the adsorption process of MB by PPAC-30C mainly consisted of the first and second stages, diaphragm diffusion and intra-particle diffusion.[40]

3.5. Adsorption isotherm

The adsorption isotherm, as shown in Fig. 4(g) and (h), can express the relationship between the adsorption amount and the adsorbent concentration at different temperatures. The adsorption amount of PPAC-30C was analysed using the Langmuir and Freundlich adsorption isotherm models at various temperatures. The physicochemical effects and energy changes of adsorption were examined based on their specific parameters. Table S3† shows that both models had a fitted R^2 greater than 0.9 in the isothermal adsorption curves at different temperatures, but the Langmuir model had a higher fitted R^2 than the Freundlich model, indicating that the Langmuir model was more suitable for representing the adsorption behaviour of MB on PPAC-30C at different temperatures. This proves that the number of active adsorption sites on the PPAC-30C surface was limited and the adsorption behaviour was monolayer adsorption.[41] The Q_0 value in this model was very close to the actual adsorption amount, which reaches 576.43 mg g^{-1}, higher than the previously reported material (Table 2). The Table S3† indicates that as temperature increases, the Q_0 value also increases, suggesting that the accumulation of MB on PPAC-30C was favoured by higher temperatures. The R_L values at all temperatures were much less than 1 and greater than 0, indicating that the adsorption of MB on PPAC-30C was favourable.[42,43]

3.6. Thermodynamic investigation

The specific thermodynamic parameters were summarized in Table S4.† From the Table S4,† ΔG^0 was negative at different temperatures, indicating that this adsorption behaviour was spontaneous and proving the feasibility of MB adsorption on PPAC.[40] With temperature rise, ΔG^0 decreased from −10.31 kJ mol^{-1} to −11.56 kJ mol^{-1}, indicating that the higher the temperature, the greater the spontaneity of adsorption and the greater the driving force to promote the adsorption reaction. $\Delta H0 = 8.39$ kJ mol^{-1} was positive, indicating that this adsorption process was a heat-absorptive reaction, which agrees with the analysis of the previous paper.[44] The value of ΔS^0 was greater than zero (62.57 J mol^{-1} K^{-1}), indicating that the adsorption behaviour was an entropy increasing phenomenon. The randomness of the reaction of the molecules at the solid–liquid interface with the active sites was improved by the increase in disorder at the solid–liquid interface, which makes MB susceptible to adsorption.[45] Generally, when ΔH^0 was less than 40 kJ mol^{-1}, the force is the van der Waals force, which can be attributed to physical adsorption. When ΔH^0 falls within the range of 50–200 kJ mol^{-1}, the mechanism involves chemical bonding and can be attributed to chemisorption.[46] In this study, the ΔH^0 of MB on phosphoric acid-activated bamboo parenchyma cell activated carbon was 8.39 kJ mol^{-1}. Thus, the primary mechanism of MB adsorption on PPAC-30C was physisorption, with some presence of chemisorption, rendering it a potential adsorbent.

3.7. Competitive adsorption

In industrial wastewater treatment, dyes are not a single component, and there are a variety of inorganic salts that influence the adsorption of dyes. To evaluate the ability of PPAC in practical applications, it is necessary to investigate the effect of coexisting ions. As illustrated in Fig. 5(a), the anion has

Table 2 Comparison of the maximum adsorption capacity of MB on PPAC-30C with other adsorbents

Materials	Experimental conditions	Q_{max} (mg g^{-1})	References
SLS-modified commercial activated carbon	328 K, pH = 5	232.5	Kuang Y.[49]
KOH-activated dragon fruit carbon	323 K, pH = 10	195.2	Jawad[50]
KOH-activated date press cake carbon	298 K, pH = 7	546.8	Heidarinejad[51]
Carbon from phosphoric acid treated eucalyptus residue	298 K, pH = 7	977	Han[26]
Magnetic activated carbon by $ZnCl_2$ activation of coconut shell	308 K, pH = 7	156.25	Yağmur[52]
Cork-based activated carbons from alkaline wastewater	293 K, pH = 5	350	Novais[53]
Carbon from phosphoric acid treated corn stigmata	298 K, pH = 7	330.5	Mbarki[54]
Bamboo chip activated carbon using KOH activation	313 K, pH = 10	305.3	Jawad[55]
PPAC-30C	T = 318 K, pH = 7	576	This study

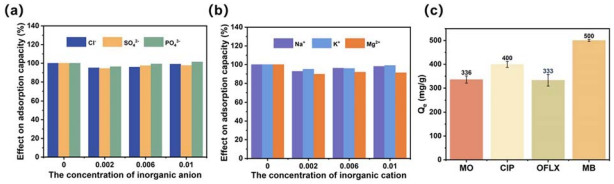

Fig. 5 Effect of interference anions (a) and cations (b) on the adsorption performance by PPAC-30C; the adsorption amount of PPAC-30C with different organic pollutants (c).

a minor impact on the adsorption of MB. This could be attributed to the negative charge on the surface of PPAC-30C under neutral conditions, which results in less involvement of the anion in the competitive adsorption with MB^+. Also, with the increase in anion concentration, the adsorption amount of MB on PPAC-30C showed a tendency to decrease and then increase, which may be due to the increase in ionic strength in the solution compressing the diffusion double layer on the surface of the adsorbent, which was conducive to the electrostatic attraction between the dye molecules and the adsorbing surface.[47] Fig. 5(b) illustrates that the adsorption of MB on PPAC-30C initially decreased and then increased with increasing cation concentration. This decrease may be due to competition between metal cations and MB cations for the limited active sites on the PPAC-30C surface. The gradual increase in the adsorption of MB during the increase in cation concentration from 0.002 mol L^{-1} to 0.01 mol L^{-1} could be attributed to the decrease in the intermolecular forces between the dye molecules with the addition of salt. MB molecules are more susceptible to dimerization and decrease in size, whereas an increase in hydrophobicity facilitates the adsorption.[33] The interfering ability of Mg^{2+} was higher than that of K^+ and Na^+, probably because it carries more charge, resulting in higher electrostatic repulsion, which makes divalent cations more susceptible to adsorption than monovalent cations.[48] In practical treatment of dye wastewater, this principle can be utilized to increase the adsorption capacity by using appropriate dye wastewater concentration.

3.8. Comparison of adsorption performance between different adsorbents and different pollutants

Comparison of the maximum adsorption capacity of MB on PPAC-30C with other adsorbents was shown in Table 2. The capacity of MB on PPAC-30C is at high level among many adsorbents. The adsorption capacity of PPAC for other pollutants (dyes and antibiotics) was investigated at the same concentration, volume and activated carbon dosage, as shown in Fig. 5(c). The equilibrium adsorption amounts were 336 mg g^{-1} of methyl orange, 400 mg g^{-1} of ciprofloxacin, 333 mg g^{-1} of ofloxacin, and 500 mg g^{-1} of methyl bromide. A comprehensive comparison can be made and it can be found that the adsorption of PPAC-30C for MB was more outstanding among a group of pollutants. Therefore, we can make a conclusion that PPAC-30C have good and relatively comprehensive adsorption performance.

3.9. Removal mechanism

Fig. 6(a) displays the XPS elemental chemical state and elemental composition curves of PPAC-30C before and after adsorption, which were used to analyse the changes of surface functional groups and binding energies resulting from the adsorption of activated carbon on phosphoric acid-activated bamboo parenchyma cells. From Fig. 6(a) and Table S5,† the C 1s, O 1s, N 1s, and P 2p peaks were from the activated carbon, whereas after adsorption of MB compared with the pristine PPAC, the O 1s and N 1s peaks are enhanced, the relative percentages of both N, O, and P were increased, the relative percentage of C was decreased, which suggests that MB has been adsorbed successfully onto the surface of PPAC-30C. In addition, the characteristic peaks of S 2s (229.0 eV) and S 2p (164.0 eV) appeared in the spectrum after adsorption, confirming that MB was adsorbed onto the phosphoric acid activated bamboo parenchyma cell activated carbon.

For the XPS profile of C 1s, four C 1s peaks were fitted at 284.8, 285.2, 286.8 and 288.9 eV, as shown in Fig. 6(b). Table S7† shows that the C 1s peak positions of activated carbon after adsorption of MB were 284.8 eV (44.0%), 285.6 eV (39.4%), 286.6 eV (12.2%), and 288.8 eV (4.4%) 38, and that adsorption resulted in a decrease around the C–C/C–H peaks, and an increase around the C–OH and C=O peaks. The binding energy may be shifted from low binding energy sites to high binding energy sites (C–OH/C=O) and this change in binding energy may be due to the decrease in electron density due to electron transfer to MB dye molecules.[56,57]

The N 1s spectra of PPAC-30C and PPAC-30C + MB were shown in Fig. 6(c). PPAC-30C was classified as –NH– (132.7 eV),

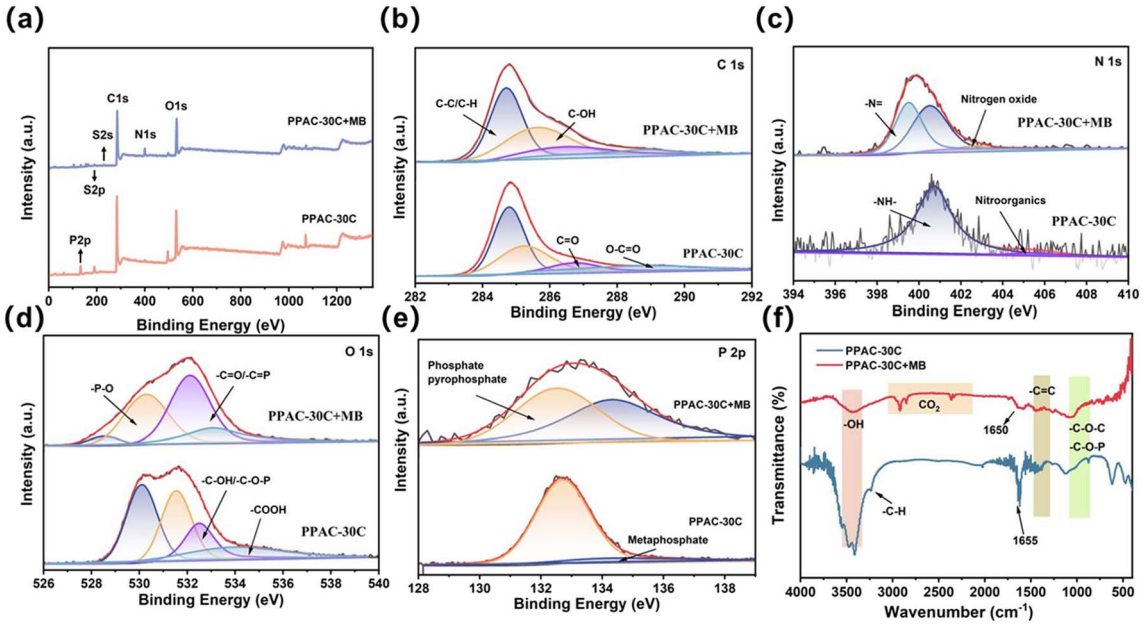

Fig. 6 XPS survey spectra (a), C 1s (b), N 1s (c), O 1s (d), and P 2p (e) XPS spectra of PPAC-30C and PPAC-30C + MB, and FTIR spectral of PPAC-30C and PPAC-30C + MB (f).

nitro-organic (134.5 eV), while after adsorption of MB, the peak of =N– (398.60 eV) appeared, with a relative content of 36.5%, which may be due to the interaction of amino group of MB molecule with This may be due to the π–π and p–π conjugation between the amino group in MB molecule and the aromatic C=C group on the surface of PPAC-30C, which resulted in the increase of the binding energy of =N–.[58]

In the O 1s XPS spectra (Fig. 6(d)), after adsorption of MB, the peaks were shifted towards –P–O (530.17 eV), –C=O/–C=P (531.67 eV), –C–OH/–C–O–P (533.24 eV), and –COOH (534.04 eV) with a decrease in the percentage of C=O peak area, indicating the active sites after adsorption of MB decrease.

Fig. 6(f) shows the interactions between PPAC-30C and MB, as explored using FTIR. After adsorption of MB, the peak at 3400 cm^{-1} decreases, indicating that hydroxyl groups may be involved in the adsorption process. The peak centred at 1633 cm^{-1} falls within the range of 1600 cm^{-1} to 1670 cm^{-1}, which suggests the aromatic C=C stretching vibration. The peaks observed at 1500–1370 cm^{-1} suggest the presence of carboxylic acid bending vibration, C–H bending vibration, and stretching aromatic C=C vibration. Each of these aromatic C=C structures contains a π electron orbital, which can generate a π–π conjugation effect with the C=C bond of methyl MB.[59] The absorption peak at 1050 cm^{-1} corresponds to the stretching vibration caused by aliphatic phosphoric acid C–O–P. The absorption peaks between 1050–1250 cm^{-1} suggest the presence of the C–O–C asymmetric stretching vibration in carboxylic esters, as well as the C–O vibration in phenol and alcohol hydroxyls. The absorption peaks at 1050–1250 cm^{-1} may indicate C–O–C asymmetric stretching vibrations in carboxylic esters and C–O vibrations in phenol and alcohol hydroxyl groups.

In addition, hydrogen bonding can occur between hydrogen on strong polar bonds and highly electronegative, lone-pair electron-containing and partially negatively charged atoms (*e.g.*, N, O, F). After hydrogen bonding forms, the position of absorption peaks in the FTIR spectrum will change. The C=O stretching vibration peak of PPAC-30C shifted to lower wavelengths after adsorption, from 1655 cm^{-1} to 1650 cm^{-1}, probably due to the combined effect of hydrogen bonding and aromatic ring conjugation on C=O. Thus, it is possible to speculate that the adsorption process of MB by phosphoric acid-activated bamboo parenchyma cells involves hydrogen bonding and π–π conjugation effects.

Based on the physical and chemical characterization and adsorption experiments, the adsorption mechanism of MB on PPAC-30C includes physical and chemical adsorption that are not independent of each other, with physical adsorption playing the major role. The adsorption process can be well described by the pseudo-second-order kinetic model and Langmuir isotherm model, indicating monolayer adsorption. The conclusion from the adsorption thermodynamic model was that the adsorption process was reversible and spontaneously absorbs heat, and the temperature rise favours the adsorption of methyl MB.

As a result, possible plausible mechanisms for the adsorption of MB on PPAC-30C were proposed as follows: (i) physical adsorption, in which both MB molecules and MB^{+} ions diffuse from the aqueous MB solution to the PPAC-30C surface and pores by membrane and molecular diffusion, and primary adsorption mechanism was pore filling; (ii) electrostatic attraction, deprotonating hydroxyl and carboxyl functional groups releases additional adsorption sites, facilitating electrostatic attraction between the negative charges on the activated carbon surface and the dye cations, thereby promoting

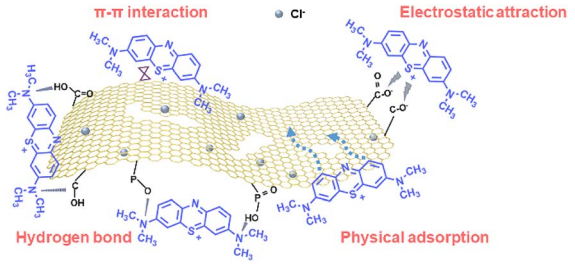

Fig. 7 Schematic representation of the mechanism of MB removal in water.

the adsorption of MB; (iii) hydrogen bonding, the functional groups on the surface of PPAC-30C form hydrogen bonding with MB, which enhances the adsorption effect of MB; (iv) π–π conjugation, the existence of an aromatic C=C structure on the surface of PPAC-30C, in which π-electron orbitals can produce a π–π conjugation effect with the C=C bonding of MB. Fig. 7 illustrates the mechanism of the PPAC-30C as analysed previously.

4. Conclusion

In this work, bamboo parenchyma cells isolated from moso bamboo were successfully synthesized and used for the adsorption of dye wastewater by activating them at 500 °C after impregnation with phosphoric acid at 10–50% concentration. The concentration of phosphoric acid affects the performance of adsorption by influencing the distribution of pore size and specific surface area of the activated carbon.

In the intermittent adsorption experiments, the adsorbent dosage, pH value and initial concentration had a significant effect on the removal of MB. A simulated pseudo-second-order kinetic model provided a more accurate description of PPAC-30C adsorption (R^2 = 0.822–0.991). The adsorption isotherm results suggested that the removal of MB was carried out *via* monolayer adsorption, which is consistent with the Langmuir model (R^2 = 0.983–0.994). The maximum adsorption capacities were 510, 556, and 578 mg g^{-1} at 298, 308, and 318 K, respectively. Furthermore, ions had less of an effect on MB removal, and the method of adsorption was reversible and self-heating. The adsorption mechanisms included physical adsorption, electrostatic interactions, hydrogen bonding and π–π conjugation effects. Overall, the multilayered and pitted structure of bamboo parenchyma cells provided active sites for the solution, resulting in a better adsorption of PPAC-30C for cationic dyes.

Author contributions

Yuxuan Yao: writing – original draft, data curation, formal analysis, conceptualization, software, project administration. Haifeng Zuo: writing – review & editing, data curation, formal analysis, conceptualization, validation, software, supervision, project administration. Yijing Liu: data curation, conceptualization. Shenghua Pang: validation, data curation, formal analysis, software. Liuqian Lan: conceptualization, software, resources. Futi Yao: methodology, validation. Yongyi Wu: methodology, project administration. Zhigao Liu: funding acquisition, data curation, conceptualization, software, resources, supervision, validation.

Conflicts of interest

All authors declare that they have no conflict of interest.

Acknowledgements

This study was financially assisted by the Guangxi Science and Technology Major Program (Guike AA23062007), the National Natural Science Foundation of China (No. 32060322) and the Innovation Training Programme of Guangxi Zhuang Autonomous Region (No. S202210593376).

References

1 M. Salehi, *Environ. Int.*, 2022, **158**, 106936.
2 M. T. Yagub, T. K. Sen, S. Afroze and H. M. Ang, *Adv. Colloid Interface Sci.*, 2014, **209**, 172–184.
3 N. Hegyesi, R. T. Vad and B. Pukánszky, *Appl. Clay Sci.*, 2017, **146**, 50–55.
4 G. D. Crozals, C. Farre, M. Sigaud, P. Fortgang, C. Sanglar and C. Chaix, *Chem. Commun.*, 2015, **51**, 4458–4461.
5 R. C. Dante, J. Trakulmututa, S. Meejoo-Smith, P. Martín-Ramos, P. Chamorro-Posada, D. Rutto and F. M. Sánchez-Arévalo, *Mater. Chem. Phys.*, 2019, **231**, 351–356.
6 I. Khan, K. Saeed, I. Zekker, B. Zhang, A. H. Hendi, A. Ahmad, S. Ahmad, N. Zada, H. Ahmad, L. A. Shah, T. Shah and I. Khan, *Water*, 2022, **14**, 242.
7 K. Piaskowski, R. Świderska-Dąbrowska and P. K. Zarzycki, *J. AOAC Int.*, 2018, **101**, 1371–1384.
8 R. G. Saratale, G. D. Saratale, J. S. Chang and S. P. Govindwar, *J. Taiwan Inst. Chem. Eng.*, 2011, **42**, 138–157.
9 V. Katheresan, J. Kansedo and S. Y. Lau, *J. Environ. Chem. Eng.*, 2018, **6**, 4676–4697.
10 Y. Xia, H. Zuo, J. Lv, S. Wei, Y. Yao, Z. Liu, Q. Lin, Y. Yu, W. Yu and Y. Huang, *J. Clean. Prod.*, 2023, **396**, 136517.
11 S. Shi, Y. Jiang, H. Ren, S. Deng, J. Sun, F. Cheng, J. Jing and Y. Chen, *Nano-Micro Lett.*, 2024, **16**, 85.
12 S. Shi, D. Zhou, Y. Jiang, F. Cheng, J. Sun, Q. Guo, Y. Luo, Y. Chen and W. Liu, *Adv. Funct. Mater.*, 2024, 2312664.
13 O. Duman, S. Tunç, T. G. Polat and B. K. Bozoğlan, *Carbohydr. Polym.*, 2016, **147**, 79–88.
14 O. Duman, T. G. Polat, C. Ö. Diker and S. Tunç, *Int. J. Biol. Macromol.*, 2020, **160**, 823–835.
15 O. Duman, T. G. Polat and S. Tunç, *J. Environ. Manage.*, 2022, **322**, 116130.
16 M. Abdullah, J. Iqbal, M. S. Ur Rehman, U. Khalid, F. Mateen, S. N. Arshad, A. G. Al-Sehemi, H. Algarni, O. A. Al-Hartomy and T. Fazal, *Chemosphere*, 2023, **317**, 137834.
17 T. Kan, V. Strezov and T. J. Evans, *Renew. Sustain. Energy Rev.*, 2016, **57**, 1126–1140.

18 H. Zuo, Y. Xia, H. Liu, Z. Liu and Y. Huang, *Ind. Crops Prod.*, 2023, **194**, 116403.
19 X. Zhang, F. Guo, Z. Yu, M. Cao, H. Wang, R. Yang, Y. Yu and L. Salmén, *Biomacromolecules*, 2022, **23**, 4053–4062.
20 Q. Lin, R. Gao, D. Li, Y. Lu, S. Liu, Y. Yu, Y. Huang and W. Yu, *npj Flexible Electron.*, 2022, **6**, 1–8.
21 C. Chen, H. Li, A. Dauletbek, F. Shen, D. Hui, M. Gaff, R. Lorenzo, I. Corbi, O. Corbi and M. Ashraf, *J. Renewable Mater.*, 2022, **10**, 605–624.
22 X. Wang, Y. Liu, J. Pu, C. Qin, S. Yao, S. Wang and C. Liang, *Ind. Crops Prod.*, 2024, **210**, 118061.
23 Z. Heidarinejad, M. H. Dehghani, M. Heidari, G. Javedan, I. Ali and M. Sillanpää, *Environ. Chem. Lett.*, 2020, **18**, 393–415.
24 S. Sonal, P. Prakash, B. Kumar Mishra and G. C. Nayak, *RSC Adv.*, 2020, **10**, 13783–13798.
25 S. Sonal, S. Acharya and B. K. Mishra, *J. Environ. Manage.*, 2022, **314**, 115009.
26 Q. Han, J. Wang, B. A. Goodman, J. Xie and Z. Liu, *Powder Technol.*, 2020, **366**, 239–248.
27 W. Liese, *The Anatomy of Bamboo Culms*, International Network for Bamboo and Rattan, Beijing, 1998.
28 S. Lu, W. Yang, M. Zhou, L. Qiu, B. Tao, Q. Zhao, X. Wang, L. Zhang, Q. Xie and Y. Ruan, *J. Colloid Interface Sci.*, 2022, **610**, 1088–1099.
29 M. Jagtoyen and F. Derbyshire, *Carbon*, 1998, **36**, 1085–1097.
30 R. Gong, K. Zhong, Y. Hu, J. Chen and G. Zhu, *J. Environ. Manage.*, 2008, **88**, 875–880.
31 M. U. Dao, H. S. Le, H. Y. Hoang, V. A. Tran, V. D. Doan, T. T. N. Le, A. Sirotkin and V. T. Le, *Environ. Res.*, 2021, **198**, 110481.
32 E. Mosaffa, R. Indravadan Patel, A. Banerjee, B. B. Basak and M. Oroujzadeh, *RSC Adv.*, 2024, **14**, 7745–7762.
33 J. Ma, F. Yu, L. Zhou, L. Jin, M. Yang, J. Luan, Y. Tang, H. Fan, Z. Yuan and J. Chen, *ACS Appl. Mater. Interfaces*, 2012, **4**, 5749–5760.
34 E. Mosaffa, A. Banerjee and H. Ghafuri, *Environ. Sci.: Water Res. Technol.*, 2023, **9**, 2643–2663.
35 V. T. Trinh, T. M. P. Nguyen, H. T. Van, L. P. Hoang, T. V. Nguyen, L. T. Ha, X. H. Vu, T. T. Pham, T. N. Nguyen, N. V. Quang and X. C. Nguyen, *Sci. Rep.*, 2020, **10**, 3634.
36 S. Bai, X. Shen, X. Zhong, Y. Liu, G. Zhu, X. Xu and K. Chen, *Carbon*, 2012, **50**, 2337–2346.
37 F. Zhao, Z. Yang, Z. Wei, R. Spinney, M. Sillanpää, J. Tang, M. Tam and R. Xiao, *Chem. Eng. J.*, 2020, **388**, 124307.
38 O. Duman, S. Tunç and T. Gürkan Polat, *Microporous Mesoporous Mater.*, 2015, **210**, 176–184.
39 O. Duman, S. Tunç, B. K. Bozoğlan and T. G. Polat, *J. Alloys Compd.*, 2016, **687**, 370–383.
40 Y. Xu, J. Chen, R. Chen, P. Yu, S. Guo and X. Wang, *Water Res.*, 2019, **160**, 148–157.
41 S. Salvestrini, *React. Kinet., Mech. Catal.*, 2018, **123**, 455–472.
42 Y. Hu, C. Pan, X. Zheng, F. Hu, L. Xu, G. Xu, Y. Jian and X. Peng, *J. Hazard. Mater.*, 2021, **401**, 123374.
43 S. Wang, N. Wang, K. Yao, Y. Fan, W. Li, W. Han, X. Yin and D. Chen, *Sci. Rep.*, 2019, **9**, 17868.
44 M. H. Dehghani, D. Sanaei, I. Ali and A. Bhatnagar, *J. Mol. Liq.*, 2016, **215**, 671–679.
45 L. Lonappan, T. Rouissi, S. Kaur Brar, M. Verma and R. Y. Surampalli, *Bioresour. Technol.*, 2018, **249**, 386–394.
46 S. Fan, J. Tang, Y. Wang, H. Li, H. Zhang, J. Tang, Z. Wang and X. Li, *J. Mol. Liq.*, 2016, **220**, 432–441.
47 X. Peng, Z. Luan and H. Zhang, *Chemosphere*, 2006, **63**, 300–306.
48 W.-C. Qian, X.-P. Luo, X. Wang, M. Guo and B. Li, *Ecotoxicol. Environ. Saf.*, 2018, **157**, 300–306.
49 Y. Kuang, X. Zhang and S. Zhou, *Water*, 2020, **12**, 587.
50 A. H. Jawad, A. Saud Abdulhameed, L. D. Wilson, S. S. A. Syed-Hassan, Z. A. ALOthman and M. Rizwan Khan, *Chin. J. Chem. Eng.*, 2021, **32**, 281–290.
51 Z. Heidarinejad, O. Rahmanian, M. Fazlzadeh and M. Heidari, *J. Mol. Liq.*, 2018, **264**, 591–599.
52 H. K. Yağmur and İ. Kaya, *J. Mol. Struct.*, 2021, **1232**, 130071.
53 R. M. Novais, A. P. F. Caetano, M. P. Seabra, J. A. Labrincha and R. C. Pullar, *J. Clean. Prod.*, 2018, **197**, 1137–1147.
54 F. Mbarki, T. Selmi, A. Kesraoui and M. Seffen, *Ind. Crops Prod.*, 2022, **178**, 114546.
55 A. H. Jawad and A. S. Abdulhameed, *Energy, Ecol. Environ.*, 2020, **5**, 456–469.
56 S. Sahu, S. Pahi, S. Tripathy, S. K. Singh, A. Behera, U. K. Sahu and R. K. Patel, *J. Mol. Liq.*, 2020, **315**, 113743.
57 B. Singh, Y. Fang, B. C. C. Cowie and L. Thomsen, *Org. Geochem.*, 2014, **77**, 1–10.
58 H. Zhang, P. Wang, Y. Zhang, B. Cheng, R. Zhu and F. Li, *RSC Adv.*, 2020, **10**, 41251–41263.
59 Z. Wu, H. Zhong, X. Yuan, H. Wang, L. Wang, X. Chen, G. Zeng and Y. Wu, *Water Res.*, 2014, **67**, 330–344.